Volume 195, issue 4, 15 February 2010 ISSN 0378-7753

ELSEVIER

JOURNAL OF
POWER
SOURCES

International Journal on the Science and Technology
of Battery, Fuel Cell and other Electrochemical Systems

Journal of Power Sources 195 (2010) 955–961

Contents lists available at ScienceDirect

Journal of Power Sources

journal homepage: www.elsevier.com/locate/jpowsour

Quantification of SOFC anode microstructure based on dual beam FIB-SEM technique

Hiroshi Iwai[a,*], Naoki Shikazono[b], Toshiaki Matsui[c], Hisanori Teshima[b], Masashi Kishimoto[a], Ryo Kishida[c], Daisuke Hayashi[a], Katsuhisa Matsuzaki[b], Daisuke Kanno[b], Motohiro Saito[a], Hiroki Muroyama[c], Koichi Eguchi[c], Nobuhide Kasagi[b], Hideo Yoshida[a]

[a] *Department of Aeronautics and Astronautics, Kyoto University, Sakyo-ku, Kyoto 606-8501, Japan*
[b] *Department of Mechanical Engineering, The University of Tokyo, Hongo 7-3-1, Bunkyo-ku, Tokyo 113-8656, Japan*
[c] *Department of Energy and Hydrocarbon Chemistry, Kyoto University, Nishikyo-ku, Kyoto 615-8510, Japan*

ARTICLE INFO

Article history:
Received 28 July 2009
Received in revised form 2 September 2009
Accepted 3 September 2009
Available online 11 September 2009

Keywords:
Solid oxide fuel cell
Anode microstructure
Three-phase boundary length
Tortuosity factor
Focused ion beam scanning electron microscopy

ABSTRACT

The three-dimensional microstructure of an SOFC anode is quantified using a dual beam focused ion beam scanning electron microscopy (FIB-SEM) system equipped with an energy dispersive X-ray spectroscopy (EDX) unit. The microstructure of the Ni–YSZ anode is virtually reconstructed in a computational field using a series of acquired two-dimensional SEM images. The three-phase boundary (TPB) density and tortuosity factors are carefully evaluated by applying two different evaluation methods to each parameter. The TPB density is estimated by a volume expansion method and a centroid method, while the tortuosity factors are evaluated by a random walk calculation and a lattice Boltzmann method (LBM). Estimates of each parameter obtained by the two methods are in good agreement with each other, thereby validating the reliability of the analysis methods proposed in this study.

1. Introduction

A solid oxide fuel cell (SOFC) is one of the most promising energy conversion devices because of its high efficiency and fuel flexibility [1]. Long-term durability is one of the most important requirements for the practical application of the SOFC system, and great efforts have been made to develop materials with high stability and electrodes with optimal microstructures. Porous Ni–zirconia cermets such as Ni–yttria stabilized zirconia (Ni–YSZ) and Ni–scandia stabilized zirconia (Ni–ScSZ) are the most commonly used anode materials in SOFCs, because their thermal expansion coefficient can match that of the electrolyte, and they can effectively extend reaction sites (three-phase boundary, TPB) with high electrocatalytic activity [2,3]. It is widely recognized that the anode microstructure has a significant impact on cell performance as well as cell durability [4–8]. For example, effects of morphology change [7–9] and dependence on starting materials and fabrication methods have been reported [10–12]. However, the quantitative relationship between the anode microstructure and the polarization resistance is not fully understood. Recently, direct measurements of 3D SOFC electrode microstructures have been performed by focused ion beam scanning electron microscopy (FIB-SEM) [13–17] and X-ray computed tomography (XCT) [18]. Through these 3D measurements, important microstructural parameters such as TPB length and tortuosity factors can be obtained. It is expected that these new methods will provide important information for quantitatively connecting the electrode microstructure to its polarization characteristics.

It seems, however, that there is little discussion on the evaluation methods to estimate TPB density and tortuosity factors using a 3D dataset, even though the accuracy of the estimation depends on the evaluation procedures. For example, it is apparent that the total TPB length would be overestimated if the lengths of TPB edge segment are simply summed because of the inevitable step-like pattern of voxel edges. Only limited descriptions can be found in literature about the calculation method of TPB length from a 3D dataset. Golbert et al. [19] counted all the voxels neighboring a TPB edge and divided this overall number by four. Suzue et al. [20] counted the cubic voxel perimeter and assumed that TPB was 20% smaller than the total value. Smith et al. [15] and Wilson and Barnett [21] estimated TPB length from 2D images by stereology. The advantage of using a 3D dataset is lost in this method and the accuracy of the TPB length estimated by stereology should also be discussed. Wilson et al. [13] and Izzo et al. [18] evaluated the tortuosity factors by solving Laplace equation with finite element

---

[*] Corresponding author. Tel.: +81 75 7535218; fax: +81 75 7535203.
E-mail address: iwai@mbox.kudpc.kyoto-u.ac.jp (H. Iwai).

0378-7753/$ – see front matter © 2009 Elsevier B.V. All rights reserved.
doi:10.1016/j.jpowsour.2009.09.005

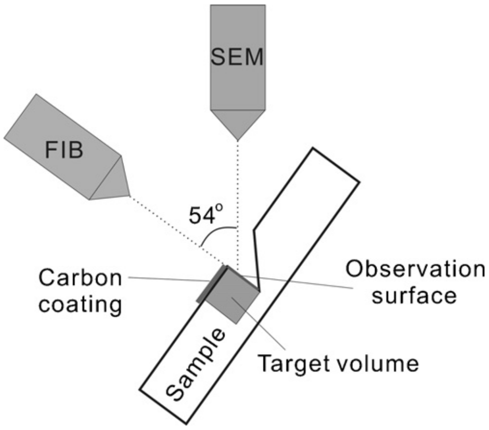

Fig. 1. Schematic diagram of FIB-SEM setting.

method (FEM) and lattice Boltzmann method (LBM), respectively. Gostovic et al. [14] and Smith et al. [15] calculated tortuosity by tracking the pore center locations and measuring the lengths of the paths. As the values of TPB length and tortuosity factors depend on the evaluation procedures, those procedures must be validated before discussing the relationship between microstructural parameters and polarization characteristics.

In the present study, the 3D microstructure of a conventional Ni–YSZ anode is quantified by dual beam FIB-SEM. An in-lens secondary electron detector is used, which provides a clear contrast between the Ni and the YSZ phases with submicron resolution. From the reconstructed 3D structure, various microstructural parameters such as volume fraction, TPB length, and tortuosity factors are quantified. We pay strong attention to the evaluation procedures for TPB length and the tortuosity factors to ensure reliability of the final estimates so that those estimates can be used to correlate microstructure with polarization characteristics in our future investigation. Two different analyzing methods are compared for the acquisition of each parameter. TPB density is estimated by the volume expansion method and the centroid method proposed in this study while the tortuosity factors are validated by the random walk calculation and the LBM-based calculation.

2. Experimental

2.1. Sample preparation

In this study, we examined the Ni–YSZ cermet anode (Ni:YSZ = 50:50 vol.%, YSZ:8 mol%Y_2O_3–ZrO_2) of conventional button cell, Ni–YSZ|YSZ|LSM. The anode material, NiO–YSZ, was mixed with polyethylene glycol, screen printed on a YSZ electrolyte, and sintered at 1400 °C for 5 h. The $(La_{0.8}Sr_{0.2})_{0.97}MnO_3$ (abbreviated as LSM) cathode was also mixed with polyethylene glycol to form slurry. It was then screen printed on the other face of the electrolyte and sintered at 1150 °C for 5 h. These button cells could be used in power generation experiments performed in laboratories. However, no power generation test was conducted on a cell examined in this study. After the anode of the test cell was reduced at 1000 °C, the cell temperature was lowered to room temperature and the anode was supplied to the FIB-SEM observation as a sample. The sample was infiltrated with epoxy resin (Marumoto Struers KK) under vacuum conditions so that the pores of the porous electrode could be easily distinguished during SEM observation. Cured sample was polished using an Ar-ion beam cross-section polisher (JEOL Ltd., SM-09010) and made available for the FIB-SEM (Carl Zeiss, NVision 40) observation.

2.2. FIB-SEM observation

Observation and quantification of the 3D microstructure of the Ni–YSZ anode are facilitated by using Kyoto University's FIB-SEM, NVision 40, equipped with a Gemini FE-SEM column (Carl Zeiss), a zeta FIB column (SIINT), and a multichannel gas injection system (SIINT). The FIB-SEM system also has EDX and electron backscattered diffraction (EBSD) units.

Fig. 1 schematically shows a typical setting for FIB-SEM observation. In this system, two beams have a coincident angle of 54°. In this study, an in-lens secondary electron detector with a typical acceleration voltage of 1–2 kV was used for carrying out the observation. A sample electrode is set up, as shown in Fig. 1. The front part of the target volume is removed by FIB milling before observation. By using the gas injection system, carbon is deposited on the surface of the target volume to protect it from undesired milling and to prevent the charging up of the observation surface.

Fig. 2(a) shows the SEM image of a sample electrode after appropriate sample preparation. FIB-SEM observation proceeds as follows: The surface of the observation area is slightly milled in the *z* direction by FIB so that a new *x*–*y* observation surface is exposed for SEM imaging. By automatically repeating this ion milling and SEM imaging sequence, known as "cut-and-see" operation in the NVision 40 system, a series of SEM images necessary for 3D structure analysis is acquired. Because image drifting is an unavoidable problem during image acquisition, and precise image alignment is essential for the quantitative analysis of the 3D microstructure, one additional procedure is required before beginning the milling and imaging sequence. To assist the latter alignment process of SEM

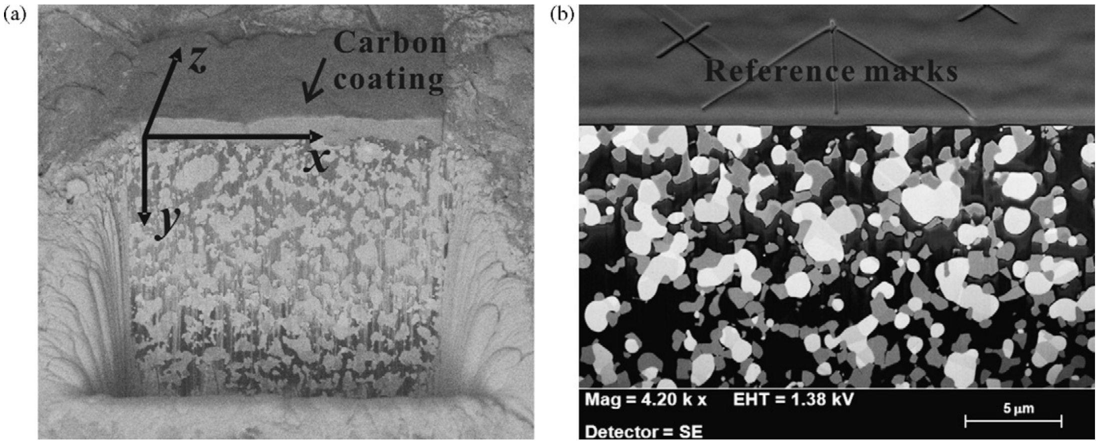

Fig. 2. (a) SEM image of sample anode before "cut-and-see" operation sequence and (b) reference marks created on the carbon coating.

Table 1
Sizes and spatial resolutions of three samples.

	x	y	z
Sample 1			
Sample dimension (μm)	26.095	10.906	4.74
Number of voxels	981	410	79
Sample 2			
Sample dimension (μm)	25.722	11.624	6.572
Number of voxels	967	437	106
Sample 3			
Sample dimension (μm)	26.341	10.768	6.048
Number of voxels	994	407	84

images, reference marks are created on the carbon layer deposited on the sample surface using FIB, as shown in Fig. 2(b). Sequential dataset acquisition by FIB-SEM is carried out at three different locations of one sample anode. The sizes and spatial resolutions of three datasets are summarized in Table 1.

2.3. 3D microstructure reconstruction

The 3D microstructure of the Ni–YSZ anode is virtually reconstructed in a computational field using 2D SEM images obtained via FIB-SEM observation. SEM images are first aligned based on the reference marks created on the carbon layer deposited on the sample surface (see Section 2.2). We found that controlling FIB milling precisely to maintain the milling direction perpendicular to the observation surface throughout the "cut-and-see" sequence in this study did not result in any noticeable image inclination. Therefore, image alignment was carried out only by parallel shifting in the *x* and *y* directions.

Separation of three phases is carried out for each SEM image. Fig. 2(b) shows that the pore region filled with epoxy resin is easily distinguished because it appears as a thick black region. On the other hand, separation of the solid part into the Ni phase and the YSZ phase requires careful consideration. EDX analysis is performed at the beginning or the end of FIB-SEM observation in order to correlate brightness with two solid phases. Fig. 3 shows an example of correlated EDX and SEM images. The Ni and YSZ phases can be clearly distinguished. Correlation obtained is applied to all the images of the same data series. Separation of the three phases is performed semi-automatically, with some manual corrections to finalize the process.

After the alignment and the phase separation processes, the dataset is ready for 3D structure reconstruction. Fig. 4 shows an example of Ni–YSZ anode microstructure reconstructed in this study.

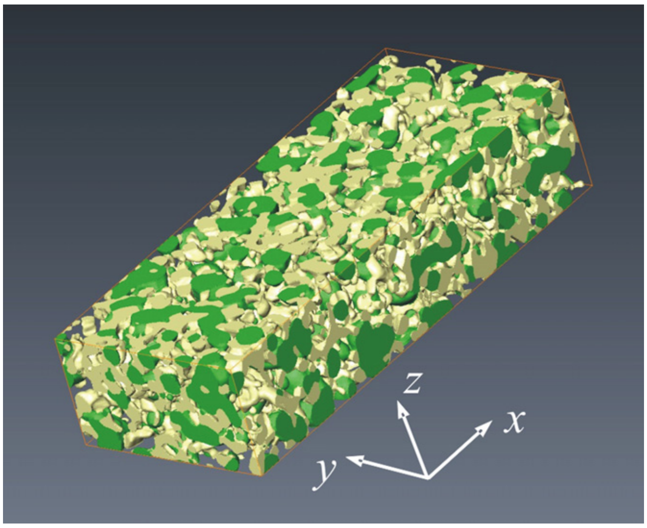

Fig. 4. Reconstructed Ni–YSZ anode microstructure (25.722 μm × 11.624 μm × 6.572 μm; green: Ni, yellow: YSZ).

3. Quantification results and discussion

Geometric parameters of the sample anode are evaluated using 3D structure data. TPB density and tortuosity factors are important geometric parameters not only for quantitatively characterizing the anode performance but also for developing reliable models for numerical simulations. It seems, however, that there is no established method to estimate TPB density and tortuosity factors for a FIB-SEM dataset, even though the accuracy of the estimation depends on the evaluation procedures. In this study, we apply two different evaluation procedures to each parameter and compare the results of each procedure in order to ensure reliability of the final estimate.

3.1. Volume fractions

The 3D reconstruction process was carried out for three sample datasets, and its results were used for the quantification study. Table 2 summarizes volume fractions, which are among the most fundamental properties, of each phase of the three samples. Because the sample anode is fabricated to be Ni:YSZ = 50:50 vol.%, the ratio of Ni and YSZ volume fractions is expected to be unity. This ratio is actually calculated to be 1.09, 1.01, and 0.94 for the three samples, respectively. We found that this variation in the values of the abovementioned ratio was not negligible; however,

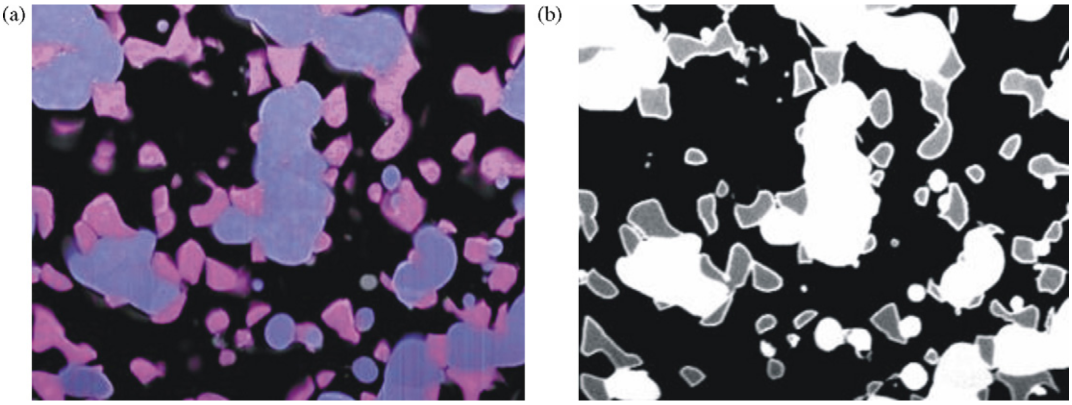

Fig. 3. (a) EDX and (b) SEM images matching for separation of three phases. Blue and red regions correspond to Ni and YSZ phases, respectively, in the EDX image.

Table 2
Volume fractions (%) of three phases.

	Ni	YSZ	Pore
Sample 1	27.4	25.1	47.5
Sample 2	25.3	25.1	49.6
Sample 3	24.5	26.0	49.5

it was still within the acceptable range. The fact that even a fundamental property such as volume fraction suffers such variation implies that a large sample size is preferred for the quantitative analysis. Increasing the sample size, however, inevitably lowers spatial resolution. The balance between the sample size and the spatial resolution is an essential problem of this method, and it is strongly related to the fabrication process of cells. In the latter sections, we consider sample 2 to be a representative sample. It was resampled to have a 62 nm × 62 nm × 62 nm cubic voxel structure, because some of the following analysis methods require such a voxel structure. The resulting sample size was 18.600 μm × 8.432 μm × 6.200 μm.

3.2. Three-phase boundary length

3.2.1. Volume expansion method

TPB forms lines in the 3D reconstructed field. If we slightly expand each phase outward in the virtual field, the overlapped regions form tube-like volumes that contain TPB lines inside. Using this method, centerlines of those tubes are taken as lines that represent TPBs, and their lengths are measured. It is worth noting that lines obtained through this method theoretically match TPBs if the spatial resolution of 3D reconstruction is sufficiently high and volume expansion is limited to be infinitely small. The validity of this method is examined by applying it to a well-defined problem. Fig. 5(a) shows a geometry adopted for a test calculation. We assume two spheres, each representing one phase, are placed in the surrounding third phase. When the two spheres are partially overlapped as shown in the figure, a circle-shape TPB is formed. The volume expansion method is applied to this problem varying its space resolution and the obtained TPB lengths are compared with the theoretical values. Fig. 5(b) shows the results of the test calculation corresponding to the geometry shown in Fig. 5(a). After conducting many test calculations by changing relative positions of the two spheres, we concluded that this method provides reasonable results for structures that have a characteristic length greater than 10 voxels. TPB density estimated by the volume expansion method is 2.487 μm μm^{-3} for the sample used in this study.

3.2.2. Centroid method

The phase of each voxel is assigned as either Ni, YSZ, or pore. If the neighboring four voxels comprise every three phases, and the phases of the diagonal voxels are not the same, the line segment surrounded by the four voxels is defined as the three-phase boundary. Then, triangles are defined by the neighboring three midpoints of the three-phase boundary segments. The three-phase boundary length is calculated as the distance between the centroids of these triangles. The total TPB length and the active TPB lengths in the x, y, and z directions are listed in Table 3. The total TPB length obtained by the centroid method is 2.556 μm μm^{-3}. The difference between the volume expansion method is less than 3%.

Although present Ni–YSZ composition (Ni:YSZ = 50:50 vol.%) is not the same as those in Refs. [13,17], total TPB densities obtained by the present methods are smaller than those reported in Ref. [13], 4.28 μm μm^{-3}, and in Ref. [17], 10.58 and 9.36 μm μm^{-3}. Present results show better agreement with the values obtained from stereology [21], i.e., 2.73 and 2.50 μm μm^{-3} for Ni:YSZ = 44:56 vol.% and 55:45 vol.%, respectively.

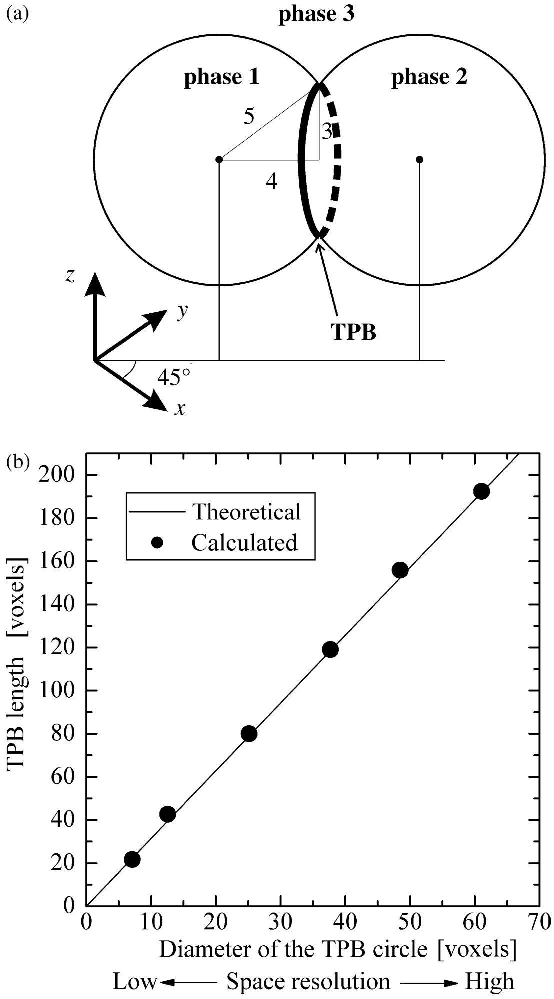

Fig. 5. Validation of TPB length obtained by applying the volume expansion method to a well-defined problem: (a) test geometry set for the validation and (b) comparison with the theoretical value at various space resolutions.

3.3. Tortuosity factor

3.3.1. Random walk calculation

Tortuosity factor can be statistically calculated from the random walk process of nonsorbing particles. As the first step of this method, a number of random walkers are randomly distributed to the pore voxels. Each walker randomly chooses one of the neighboring voxels as its possible location in the next time step. If the selected neighboring voxel represents the pore part, the walker migrates to that voxel. If the selected voxel is a solid voxel, the walker stays at the current voxel and waits for next time step. In this procedure, neither absorption nor desorption is taken into account. When repeating this procedure, the mean square displacement of random walkers is calculated as follows:

$$\langle r^2(t)\rangle = \frac{1}{n}\sum_{i=1}^{n}(\{x_i(t)-x_i(0)\}^2 + \{y_i(t)-y_i(0)\}^2 + \{z_i(t)-z_i(0)\}^2) \quad (1)$$

where n is the total number of random walkers and $\langle\rangle$ denotes an ensemble average. Because mean square displacement $\langle r^2\rangle$ is proportional to time, the diffusion coefficient, D, of nonsorbing species

Table 3
Three-phase boundary length by centroid method.

	TPB length (μm μm^{-3})
Total TPB	2.556 (100%)
Active TPB ($x = 0$ μm: electrolyte, $x = 18.6$ μm: current collector)	1.539 (60.2%)
Active TPB ($x = 0$ μm: current collector, $x = 18.6$ μm: electrolyte)	1.067 (41.7%)
Active TPB ($y = 0$ μm: electrolyte, $y = 8.43$ μm: current collector)	1.400 (54.8%)
Active TPB ($y = 0$ μm: current collector, $y = 8.43$ μm: electrolyte)	1.399 (54.7%)
Active TPB ($z = 0$ μm: electrolyte, $z = 6.2$ μm: current collector)	1.647 (64.4%)
Active TPB ($z = 0$ μm: current collector, $z = 6.2$ μm: electrolyte)	1.659 (64.9%)

is related to the time-derivative of $\langle r^2 \rangle$, as follows:

$$D = \frac{1}{6}\frac{\mathrm{d}\langle r^2(t)\rangle}{\mathrm{d}t} \tag{2}$$

The mean square displacement in a porous medium, $\langle r^2 \rangle_{\text{Pore}}$, takes a lower value than that obtained in a free space because of the obstruction effects of solids. Considering that the effective diffusion coefficient, D^{eff}, is expressed as

$$D^{\text{eff}} = V_{\text{Pore}}\frac{1}{6}\frac{\mathrm{d}\langle r^2(t)\rangle_{\text{Pore}}}{\mathrm{d}t} \tag{3}$$

the degree of reduction is measured quantitatively by the tortuosity factor as follows [22,23]:

$$\tau_{\text{Pore}} = \frac{D}{D^{\text{eff}}/V_{\text{Pore}}} = \frac{\mathrm{d}\langle r^2(t)\rangle}{\mathrm{d}t} \bigg/ \frac{\mathrm{d}\langle r^2(t)\rangle_{\text{Pore}}}{\mathrm{d}t} \tag{4}$$

Note that tortuosity factor is different from tortuosity, which is defined as the ratio of the average winded pore length to the thickness of the porous material [24]. Tortuosity factor is much more important than tortuosity because the former is directly related to effective diffusivity or conductivity.

When the porous medium has an anisotropic pore structure, the mean square displacement $\langle r^2 \rangle$ may be divided into directional mean square displacements, $\langle x^2 \rangle$, $\langle y^2 \rangle$, and $\langle z^2 \rangle$, as follows:

$$\langle x^2(t)\rangle = \frac{1}{n}\sum_{i=1}^{n}\{x_i(t) - x_i(0)\}^2 \tag{5}$$

$$\langle y^2(t)\rangle = \frac{1}{n}\sum_{i=1}^{n}\{y_i(t) - y_i(0)\}^2 \tag{6}$$

$$\langle z^2(t)\rangle = \frac{1}{n}\sum_{i=1}^{n}\{z_i(t) - z_i(0)\}^2 \tag{7}$$

Because Eqs. (5), (6) and (7) are obtained in three directions, tortuosity factors have three different values, corresponding to the x, y, and z directions.

If there are isolated pores, pores connected to the computational domain surface boundaries are extracted from stacked images as "effective pores". Isolated pores are excluded from the calculation because they do not contribute to the gas diffusion and may cause an overestimation of the tortuosity factor. In this case the volume fraction of the effective pores, $V_{\text{Pore,eff}}$, is used in Eq. (3) and the tortuosity factor is calculated as follows:

$$\tau_{\text{Pore}} = \frac{D}{D^{\text{eff}}/V_{\text{Pore}}} = \frac{V_{\text{Pore}}}{V_{\text{Pore,eff}}}\frac{\mathrm{d}\langle r^2(t)\rangle}{\mathrm{d}t} \bigg/ \frac{\mathrm{d}\langle r^2(t)\rangle_{\text{Pore}}}{\mathrm{d}t} \tag{8}$$

In order to obtain an accurate value of the tortuosity factor, a long time step and a large number walker are necessary. However, as the time step proceeds, random walkers may go out of the stacked images. A mirror symmetric boundary condition is applied to solve this problem, because it guarantees connectivity of pore structure across boundaries. The calculation is carried out for 10,000,000 time steps with 100,000 random walkers. Data obtained during the first 5,000,000 steps are omitted in the calculation of the diffusion coefficient because walkers have not yet experienced the porous solid structure at the early stage of the random walk. We use "SIMD-oriented Fast Mersenne Twister (SFMT)" as a high performance pseudorandom number generator in this method to meet the requirement for a large-scale random number.

The accuracy of this method is examined by applying it to a well-defined problem shown in Fig. 6(a). An inclined straight path is formed in the computational domain. The tortuosity factor in x-direction, τ_x, can theoretically be calculated in the ideal case as $\tau_x = 1 + \tan^2\theta$ where θ is the inclination angle. τ_x is calculated varying the path width, W, and the inclination angle. The results are compared with the theoretical values in Fig. 6(b). The discrepancy from the theoretical value becomes large at a large inclination angle

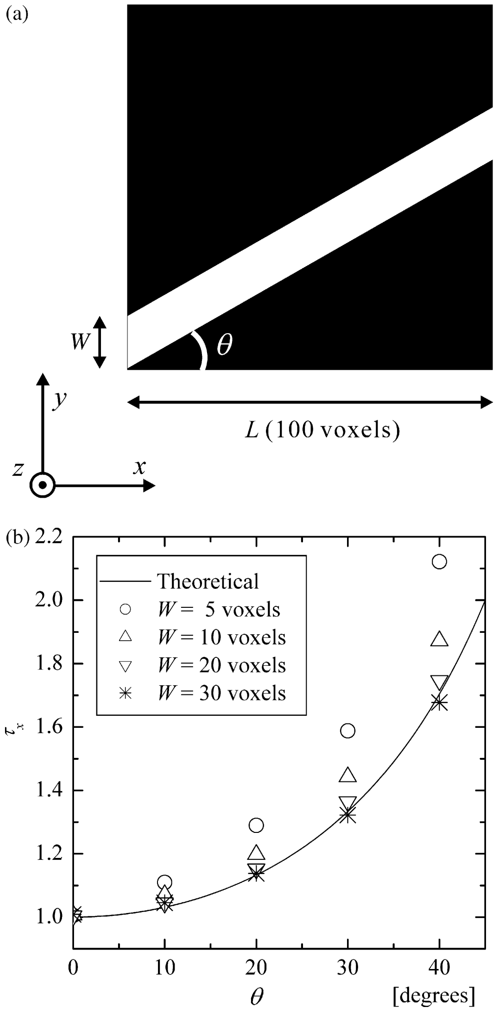

Fig. 6. Validation of tortuosity factors obtained through the random walk calculation for a well-defined problem: (a) the problem settings for the validation and (b) comparison with the theoretical value under various conditions.

when W is small. We can see a tendency that the tortuosity factor is overestimated when the space resolution is insufficient. The requirement for the space resolution is severer than what required for the TPB length estimation. We concluded that this method provides reasonable results for structures that have a characteristic length greater than 20 voxels.

The calculation results of this method are shown in the next section together with the results of LBM-based calculation.

3.3.2. Lattice Boltzmann method (LBM)-based calculation

Assuming that Ni and YSZ are perfect electronic and ionic conductors, the gaseous, electronic, and ionic diffusion equations are solved inside each of the obtained 3D structures of Ni, YSZ, and pore phases as follows:

$$\frac{\partial}{\partial x_\alpha}\left(D\frac{\partial C}{\partial x_\alpha}\right)=0 \tag{9}$$

$$\frac{\partial}{\partial x_\alpha}\left(\frac{\sigma_{\mathrm{el}}}{F}\frac{\partial \eta_{e^-}}{\partial x_\alpha}\right)=0 \tag{10}$$

$$\frac{\partial}{\partial x_\alpha}\left(\frac{\sigma_{\mathrm{io}}}{2F}\frac{\partial \eta_{\mathrm{O}^{2-}}}{\partial x_\alpha}\right)=0 \tag{11}$$

where x_α represents x, y, z directions; C is concentration; D is diffusion coefficient; η is electrochemical potential; σ is conductivity; and F is Faraday's constant. The lattice Boltzmann method (LBM) [20] is used to solve Eqs. (9), (10) and (11). The LB equation with the LBGK model in the collision term is expressed as follows:

$$f_i(\mathbf{x}+\mathbf{c}_i\Delta t, t+\Delta t)=f_i(\mathbf{x},t)-\frac{1}{t^*}[f_i(\mathbf{x},t)-f_i^{\mathrm{eq}}(\mathbf{x},t)]+w_i\Delta t \tag{12}$$

In Eq. (12), f_i represents the velocity distribution function with velocity $\mathbf{c}_i$ in the ith direction, and f_i^{eq} is the Maxwellian local equilibrium distribution. For the 3D LBM simulation, the D3Q15 (i = 1–15) or D3Q19 (i = 1–19) models are commonly used. However, it has been shown that in case of simple diffusion simulation, the D3Q6 (i = 1–6) model can be used with only a slight loss of accuracy [25]; therefore, we have used the D3Q6 model in our current study. The relaxation time, t^* = 0.99, is fixed for all simulations. Dirichlet boundary conditions are applied at the boundary surfaces. From the LBM calculation, we can obtain the effective diffusion coefficient D^{eff} of the gas phase as well as the respective effective conductivities of the Ni and YSZ phases, $\sigma_{\mathrm{Ni}}^{\mathrm{eff}}$ and $\sigma_{\mathrm{YSZ}}^{\mathrm{eff}}$. Because Eqs. (9), (10) and (11) are similar, tortuosity factors for each phase, τ_{Pore}, τ_{Ni}, and τ_{YSZ}, are defined as follows:

$$D^{\mathrm{eff}}=\frac{V_{\mathrm{Pore}}}{\tau_{\mathrm{Pore}}}D \tag{13}$$

$$\sigma_{\mathrm{el}}^{\mathrm{eff}}=\frac{V_{\mathrm{Ni}}}{\tau_{\mathrm{Ni}}}\sigma_{\mathrm{el}} \tag{14}$$

$$\sigma_{\mathrm{io}}^{\mathrm{eff}}=\frac{V_{\mathrm{YSZ}}}{\tau_{\mathrm{YSZ}}}\sigma_{\mathrm{io}} \tag{15}$$

where V_{Pore}, V_{Ni}, and V_{YSZ} are the volume fractions of the Pore, Ni, and YSZ phases, respectively.

Calculated tortuosity factors for the three phases are summarized in Table 4 together with the values estimated by the random walk method. The tortuosity factors evaluated in these methods only include geometrical aspects. Other effects such as reaction or diffusion on the surface of electrochemically active nickel are not considered. The results afforded by both methods are in good agreement with each other (less than 3% difference). The values for the pore in Table 4 are also close to the values reported in Wilson et al. [13] (τ_x, τ_y, τ_z) = (2.1, 2.2, 1.9). To the authors' knowledge, this is the first report on the tortuosity factors of the solid phases, τ_{Ni} and τ_{YSZ}. Cross-sectional areas normal to the x, y, and z directions are 52.3 μm^2, 115.3 μm^2, and 156.8 μm^2, respectively. As shown in Table 4, the tortuosity factors of the solid phases, τ_{Ni} and τ_{YSZ}, have large values for the x and y directions. On the other hand, τ_{Pore} has nearly the same values for all the three directions. We conclude that the winded electronic and ionic paths are disconnected at the side boundaries for the x and y directions. From Table 4, it is evident that the processed volume size is not sufficiently large for evaluating the effective conductivities of the solid phases for the present sample.

Table 4
Anisotropic tortuosity factors calculated by two methods.

	Random walk	Lattice Boltzmann method
τ_{Pore}		
x	2.05	2.03
y	1.99	2.06
z	1.78	1.83
τ_{Ni}		
x	22.10	21.68
y	29.46	29.45
z	6.91	6.94
τ_{YSZ}		
x	27.89	27.66
y	14.95	14.82
z	9.86	9.84

The validated TPB length and tortuosity factors will be coupled with the numerical simulation in the future work, which will provide a quantitative relationship between microstructure and anode polarization.

4. Conclusions

The three-dimensional microstructure of a Ni–YSZ anode was quantified by dual beam FIB-SEM. An in-lens secondary electron detector was used, which provided clear contrast between the Ni and YSZ phases as well as submicron resolution. The reconstructed three-dimensional structure was used to quantify microstructural parameters such as the volume fraction, TPB length, and tortuosity factors. TPB density was estimated by the volume expansion method and the centroid method proposed herein; the results matched well—less than 3% difference was found between the two sets of results. This proves the reliability of the two analysis methods for TPB density proposed. The tortuosity factors were evaluated by the random walk calculation and the LBM-based calculation. The results for the three phases afforded by both methods matched well—differences were less than 3%. This validates the two analysis methods for the tortuosity factors adopted in this study. However, it was also revealed that the volume of the sample used in this study was not sufficient for a quantification of the effective conductivities of Ni and YSZ. The next step will be coupling the validated TPB length and tortuosity factors with the numerical simulation, which will provide a quantitative relationship between microstructure and anode polarization.

Acknowledgments

This work was supported by the New Energy and Industrial Technology Development Organization (NEDO) under the Development of System and Elemental Technology on Solid Oxide Fuel Cell (SOFC) Project.

References

[1] S.C. Singhal, K. Kendall, High Temperature Solid Oxide Fuel Cells, Elsevier, 2002.
[2] M. Mogensen, S. Skaarup, Solid State Ionics 86–88 (1996) 1151–1160.
[3] N.Q. Minh, J. Am. Ceram. Soc. 76 (1993) 563–588.

[4] H. Koide, Y. Someya, T. Yoshida, T. Maruyama, Solid State Ionics 132 (2000) 253–260.
[5] A. Atkinson, S. Barnett, R.J. Gorte, J.T.S. Irvine, A.J. Mcevoy, M. Mogensen, S.C. Singhal, J. Hohs, Nat. Mater. 3 (2004) 17–27.
[6] H. Abe, K. Murata, T. Fukui, W.-J. Moon, K. Kaneko, M. Naito, Thin Solid Films 496 (2006) 49–52.
[7] T. Fukui, K. Murata, S. Ohara, H. Abe, M. Naito, K. Nogi, J. Power Sources 125 (2004) 17–21.
[8] H. Itoh, T. Yamamoto, M. Mori, T. Horita, N. Sakai, H. Yokokawa, M. Dokiya, J. Electrochem. Soc. 144 (2) (1997) 641–646.
[9] W.Z. Zhu, S.C. Deevi, Mater. Sci. Eng. A362 (2003) 228–239.
[10] Y.-J. Leng, S.-H. Chan, K.-A. Khor, S.-P. Jiang, P. Cheang, J. Power Sources 117 (2003) 26–34.
[11] S.-D. Kim, H. Moon, S.-H. Hyun, J. Moon, J. Kim, H.-W. Lee, Solid State Ionics 177 (2006) 931–938.
[12] J.-H. Yu, G.-W. Park, S. Lee, S.-K. Woo, J. Power Sources 163 (2007) 926–932.
[13] J.R. Wilson, W. Kobsiriphat, R. Mendoza, H.-Y. Chen, J.M. Hiller, D.J. Miller, K. Thornton, P.W. Voorhees, S.B. Adler, S. Barnett, Nat. Mater. 5 (2006) 541–544.
[14] D. Gostovic, J.R. Smith, D.P. Kundinger, K.S. Jones, E.D. Wachsman, Electrochem. Solid-State Lett. 10 (12) (2007) B214–B217.
[15] J.R. Smith, A. Chen, D. Gostovic, D. Hickey, D.P. Kundinger, K.L. Duncan, R.T. DeHoff, K.S. Jones, E.D. Wachsman, Solid State Ionics 180 (2009) 90–98.
[16] J.R. Wilson, M. Gameiro, K. Mischaikow, W. Kalies, P. Voorhees, S. Barnett, Microsc. Microanal. 15 (2009) 71–77.
[17] P.R. Shearing, J. Golbert, R.J. Chater, N.P. Brandon, Chem. Eng. Sci. 64 (2009) 3928–3933.
[18] J.R. Izzo Jr., A.S. Joshi, K.N. Grew, W.K.S. Chiu, A. Tkachuk, S.H. Wang, W. Yun, J. Electrochem. Soc. 155 (5) (2008) B504–B508.
[19] J. Golbert, C.S. Adjiman, N.P. Brandon, Ind. Eng. Chem. Res. 47 (2008) 7693–7699.
[20] Y. Suzue, N. Shikazono, N. Kasagi, J. Power Sources 184 (2008) 52–59.
[21] J.R. Wilson, S. Barnett, Electrochem. Solid-State Lett. 11 (2008) B181–B185.
[22] Y. Watanabe, Y. Nakashima, Comput. Geosci. 28 (2002) 583–586.
[23] Y. Nakashima, S. Kamiya, J. Nucl. Sci. Technol. 44 (2007) 1233–1247.
[24] N. Epstein, Chem. Eng. Sci. 44 (1989) 777–779.
[25] Th. Zeiser, P. Lammers, E. Klemm, Y.W. Li, J. Bernsdorf, G. Brenner, Chem. Eng. Sci. 56 (2001) 1697–1704.